PERFORMANCE ANALYSIS AND PRELIMINARY EXPERIMENTAL VERIFICATION OF A COHERENT OPTICAL RECEIVER FOR PPM SIGNALS IN THE PRESENCE OF ATMOSPHERIC TURBULENCE

Michela Muñoz Fernández[1,2], Victor A. Vilnrotter[2]

[1]California Institute of Technology, 1200 E. California Blvd., Pasadena, CA 91125,U.SA., michela@caltech.edu
[2]Jet Propulsion Laboratory, 4800 Oak Grove Dr., Pasadena, CA 91109, U.S.A., Victor.Vilnrotter@jpl.nasa.gov

ABSTRACT

We present the performance analysis and experimental verification of a coherent free-space optical communications system in the presence of simulated atmospheric turbulence. Bit Error Rate (BER) performance is analyzed, and laboratory equipment and experimental setup used to carry out these experiments at the Jet Propulsion Laboratory are described. The key components include two lasers operating at 1064 nm wavelength for use with coherent detection, a 16 element (4X4) focal plane detector array, and data acquisition and signal processing assembly needed to sample and collect the data and analyze the results. The detected signals are combined using the least-mean-square (LMS) algorithm. Convergence of the algorithm for experimentally obtained signal tones in the presence of atmospheric turbulence is demonstrated.

1. INTRODUCTION

Laser communications performance is affected by the atmosphere as it is a dynamic and imperfect medium. Atmospheric channel effects include fluctuations in the signal amplitude, phase, and attenuation. However, space and ground based optical communications offer potential advantages in bandwidth over traditional RF communications and conventional microwave technology. Small beam divergence, small size, and large information bandwidth due to operation at a higher frequency are all advantages of a laser system. Transmitters and receivers are smaller and lighter for a specified distance; laser requires lower power for a given distance and power; and lasers provide higher security and greater resistance to interference.

The research described in this publication was carried out by the Jet Propulsion Laboratory, California Institute of Technology, under a contract with the National Aeronautics and Space Administration.

Optical receivers can be divided into two basic types [1]: power detecting, direct detection or noncoherent receivers, and heterodyning or (spatially) coherent receivers. The simplest implementation is achieved with direct detection, where the lens system and photodetector operate to detect the instantaneous power in the collected field as it arrives at the receiver. Intensity modulation with direct detection is currently used for optical communications systems. Under ideal transmission and detection conditions, the probability of detecting n photons in a pulse train having an average of K_S photons per pulse obeys the Poisson distribution [1,2]

$$p(n) = \frac{K_S^n e^{-K_S}}{n!}. \quad (1)$$

The probability of an erasure is defined as the detection of no photons during the pulse, and is given by

$$P_E = \exp(-K_S). \quad (2)$$

An average of 21 detected photons per pulse would be needed to achieve an erasure probability of 10^{-9}. This limit is rarely reached since it assumes no dark or background counts whatsoever in the receiver. In the presence of background radiation, performance of direct detection receivers degrades significantly, as shown in [2]. One way to overcome the effects of background radiation is to use coherent detection. With coherent detection, the local oscillator (LO) mixes with the modulated wave at the photodetector. If the LO (E_L) is at the same wavelength as the received optical signal (E_S), and in addition is in phase with the optical carrier, the detection is called homodyne detection. If the frequencies of the LO and received signal are different, then it is called heterodyne detection. The heterodyne detector converts phase changes in the optical carrier to phase changes in the optical intensity, which are reproduced in the detected current waveform. The following analysis shows how the heterodyne scheme permits detection of the incoming signal beam. If the beams are spatially well aligned, there is optical interference on the photodetector surface, resulting in the intensity

$$I \propto (E_S + E_L)^2. \quad (3)$$

This inherent squaring operation at the photodetector produces a detector current at the intermediate frequency which contains the signal modulation. If the carrier and local oscillator beams are aligned perpendicular to the photodetector surface, the expression of the field incident on the detector is

$$E(t) = E_S(t)\cos[\omega_S t + \phi_S] + E_L(t)\cos[\omega_L t + \phi_L]. \quad (4)$$

The photodetector output current is proportional to the detector responsivity and the optical intensity. The responsivity [6] is given by

$$\Re = \frac{e\eta_q}{h\nu} \quad (amps/Watt), \quad (5)$$

where e is the electronic charge, η_q is the detector quantum efficiency, h is Planck's constant and $\nu = \omega/2\pi$ is the optical frequency. Therefore, the detector output current is

$$i(t) = \frac{e\eta_q}{2h\nu} E^2(t), \quad (6)$$

and

$$E^2(t) = [E_s(t)\cos(\omega_s t + \phi_S) + E_L(t)\cos(\omega_L t + \phi_L)]^2. \quad (7)$$

High frequency intensity components that oscillate at twice the optical carrier frequency are eliminated from the receiver as that frequency is much greater than the frequency response of the detector [4]. Therefore, we can write the intensity that the detector responds to as

$$E^2(t) = \frac{1}{2}E_L^2(t) + \frac{1}{2}E_S^2(t) + E_L(t)E_S(t)\cos[(\omega_L - \omega_S)t + \phi_L - \phi_S]. \quad (8)$$

The detected current is proportional to the average optical intensity, where the average is taken over a time interval long compared to the optical period, but short compared to the period of the IF.

If the local oscillator power is much greater than the signal power, the second term of Eq. (8) can be neglected. The first term represents a large and continuous signal that carries no information but generates a shot noise contribution. The third term represents the signal modulation. If the signal is coupled to a detector of responsivity $\Re$ and ac-coupled to eliminate the local oscillator signal, then we can write

$$i(t) \propto 2E_L(t)E_s(t)\cos[(\omega_L - \omega_s)t + \phi_L - \phi_s)]. \quad (9)$$

In coherent communications the optical frequency and the phase of the signal relative to the local oscillator are preserved. For the shot-noise limited case, when the effects of dark current and thermal noise are eliminated by increasing the optical power, the resulting signal-to-noise ratio [5] for heterodyne detection is

$$SNR = \frac{P_{signal}}{P_{noise}} = \frac{\eta_q P_S}{h\nu\Delta\nu}. \quad (10)$$

Therefore, the minimum detectable signal (signal input power leading to an output signal-to-noise ratio of 1) is

$$(P_S)_{\min} = \frac{h\nu\Delta\nu}{\eta_q}. \quad (11)$$

In the case of homodyne detection, the signal-to-noise ratio [6] is

$$SNR = 2\frac{\eta_q P_S}{h\nu\Delta\nu}, \quad (12)$$

and for direct detection [6], the SNR becomes

$$SNR = \frac{1}{2}\frac{\eta_q P_S}{h\nu\Delta\nu}. \quad (13)$$

Note that shot-noise limited SNR obtained in homodyne detection is a factor of two (3dB) greater than that of heterodyne receiver and a factor of four (6dB) better than the SNR of a direct detection system.

With heterodyne and homodyne optical detection, quantum-limited performance can theoretically be obtained, and receiver sensitivities on the order of 10-20 dB higher than direct detection systems are possible under high background conditions [7].

2. PERFORMANCE ANALYSIS OF A COHERENT OPTICAL RECEIVER FOR M-ARY PPM SIGNALS

When coherent detection is used, digital bits can be encoded directly on the phase or frequency of the laser carrier itself. The received modulated laser carrier can be translated to a lower RF frequency, where the digital modulation can be decoded using standard decoding techniques [8]. In the heterodyne detection system examined, pulse position modulation (PPM) is used. PPM is a form of block encoding in which bits are transmitted in blocks instead of one at a time [8]. Optical block encoding is achieved by converting each block of k bits into one of $M=2^k$ optical fields of transmission. At the receiver end, decoding of each block is performed by determining which one of the M fields is received per block time. For the PPM case, a PPM frame contains M slots and an optical pulse is placed in one of those M slots. The data word is determined based on the position of the optical pulse in

the frame. The receiver decides on the basis of maximum likelihood symbol detection; it selects the slot with the greatest energy and the symbol that contains a signal pulse in that slot location is declared to be the transmitted symbol.

If A is the aperture of the detector, $\alpha=\eta_q/h\upsilon$, and $E_L>>E_S$, from Eq. (10) and [1] the resulting intensity counting rate process of the photodetector is $\alpha AE_L^2+\alpha A2E_SE_L\cos[(\omega_L-\omega_s)t+\phi_L-\phi_s)]$. We assume that local power alone sets the shot noise level of spectral level $N_S/2$.

Under shot-noise limited conditions, and after filtering out the DC term, the detector can be modeled as:

$$r(t)=s(t)+n(t). \tag{14}$$

where $n(t)$ is a Gaussian noise process of spectral level $N_S/2=\alpha AE_L^2$. The variance of the shot-noise is calculated by integrating for τ seconds (duration of the PPM pulse) resulting in [1]: $\sigma_S^2=\alpha AE_L^2\tau$. The value of the signal for homodyne detection is also obtained by integrating for τ seconds over the signal slot resulting in $E_SE_L\alpha A\tau$. For homodyne detection: $\omega_L=\omega_s$ and $\phi_L=\phi_s$.

The signal-to-noise ratio is therefore

$$SNR=\frac{P_{signal}}{P_{noise}}=\frac{\left[2E_SE_L\alpha A\tau\right]^2}{\alpha AE_L^2\tau}=4\alpha AE_S^2\tau=4K_S, \tag{15}$$

where $K_S=\alpha AE_S^2\tau$ is the average number of signal photons over the slot duration. For the case of heterodyne detection, the frequencies are not equal $(\omega_L\neq\omega_s)$ and the signal becomes

$$s(t)=\alpha A2E_SE_L\cos[(\omega_L-\omega_s)t)], \tag{16}$$

with rms value $\frac{2}{\sqrt{2}}E_SE_L\alpha A\tau=\sqrt{2}E_SE_L\alpha A\tau$.

This results in the signal-to-noise ratio for heterodyne detection

$$SNR=\frac{\left[\sqrt{2}E_SE_L\alpha A\tau\right]^2}{\alpha AE_L^2\tau}=2\alpha AE_S^2\tau=2K_S. \tag{17}$$

The strong local field generates a high count rate at the detector output, which gives rise to Gaussian shot noise. Therefore, heterodyne detector outputs are assumed to be Gaussian processes [9, 12] with the signal term corresponding to the modulated carrier, and shot noise components considered as additive Gaussian noise with the spectral level given above. As a result, the photodetected field can be modeled as a Gaussian process, with mean $2E_SE_L\alpha A\tau$ for homodyne detection and $\sqrt{2}E_SE_L\alpha A\tau$ for heterodyne detection, and variance in both cases $\sigma_S^2=\alpha AE_L^2\tau$. The probability density can therefore be written as $p(x)=\frac{1}{\sqrt{2\pi\sigma^2}}e^{-(x-\eta)^2/2\sigma^2}$ where η is a mean value due to the signal energy.

The probability of correct PPM detection is the probability that one Gaussian random variable with mean η (corresponding to the signal slot) exceeds (M-1) other zero-mean Gaussian random variables (corresponding to the noise slots). As PPM signals are a type of orthogonal signals, for the homodyne detection case the probability of correct symbol detection $P(SC)$ can be expressed as [10], [11]

$$P(SC)=\int_{-\infty}^{+\infty}\frac{1}{\sqrt{2\pi(\alpha E_L^2A\tau)}}e^{\frac{(x-2\alpha E_LE_SA\tau)^2}{2(\alpha E_L^2A\tau)}}dx\left[\int_{-\infty}^{x}\frac{1}{\sqrt{2\pi(\alpha E_L^2A\tau)}}e^{\frac{-y^2}{2(\alpha E_L^2A\tau)}}dy\right]^{M-1}, \tag{18}$$

where $\eta=2\alpha E_SE_LA\tau$.

With the change of variables

$z=\frac{y}{\sqrt{\alpha E_L^2A\tau}}$ $dz=\frac{dy}{\sqrt{\alpha E_L^2A\tau}}$, and noting that when $y=x$, $z=\frac{x}{\sqrt{\alpha E_L^2A\tau}}$

the following simplified equation is obtained

$$P(SC)=\int_{-\infty}^{+\infty}\frac{1}{\sqrt{2\pi(\alpha E_L^2A\tau)}}e^{\frac{(x-2\alpha E_LE_SA\tau)^2}{2(\alpha E_L^2A\tau)}}dx\left[\int_{-\infty}^{\sqrt{\alpha E_L^2A\tau}}\frac{1}{\sqrt{2\pi}}e^{-z^2/2}dz\right]^{M-1}. \tag{19}$$

Then with another change of variables:

$w=\frac{x}{\sqrt{\alpha E_L^2A\tau}}$ $dw=\frac{dx}{\sqrt{\alpha E_L^2A\tau}}$, we get

$$P(SC)=\int_{-\infty}^{+\infty}\frac{1}{\sqrt{2\pi}}e^{\frac{\left(w-\sqrt{4\alpha E_S^2A\tau}\right)^2}{2}}dw\left[\int_{-\infty}^{w}\frac{1}{\sqrt{2\pi}}e^{-\frac{z^2}{2}}dz\right]^{M-1} \tag{20}$$

$$=\int_{-\infty}^{+\infty}\frac{1}{\sqrt{2\pi}}e^{\frac{\left(w-\sqrt{4K_S}\right)^2}{2}}dw\left[\int_{-\infty}^{w}\frac{1}{\sqrt{2\pi}}e^{-\frac{z^2}{2}}dz\right]^{M-1},$$

or

$$P(SC)=\int_{-\infty}^{+\infty}\frac{1}{\sqrt{2\pi}}e^{\frac{\left(w-\sqrt{4K_S}\right)^2}{2}}dw\left[1-Q(w)\right]^{M-1}, \tag{21}$$

where $Q(w)=\int_x^{\infty}\frac{1}{\sqrt{2\pi}}e^{-z^2/2}dz.$

Similarly, the probability of count symbol detection for the heterodyne case becomes

$$P(SC)=\int_{-\infty}^{+\infty}\frac{1}{\sqrt{2\pi}}e^{\frac{\left(w-\sqrt{2K_S}\right)^2}{2}}dw\left[1-Q(w)\right]^{M-1}. \tag{22}$$

Therefore the probability of correct symbol detection for the signal slot can be viewed as a Gaussian random variable with mean equal to the corresponding SNR and unit noise variance

$$p_{SIGNAL\ SLOT}(x) = \frac{1}{\sqrt{2\pi}} e^{-(x-\sqrt{SNR})^2/2}, \quad (23)$$

with $SNR = 4K_S$ for homodyne detection and $SNR = 2K_S$ for heterodyne detection. For the remaining slots with no signal, the process could be modeled as a Gaussian random variable with zero mean and unit variance

$$p_{NOISE\ SLOT}(x) = \frac{1}{\sqrt{2\pi}} e^{-x^2/2} . \quad (24)$$

These expressions are accurate under strong local field condition and negligible background radiation. If equal a-priori transmission probabilities are assumed for each symbol, the probability of symbol error [1] can be expressed as

$$P(SE) = 1\text{-}P(SC). \quad (25)$$

Finally, to obtain the bit error probability for homodyne detection [1] as

$$P_e=[(M/2)/(M\text{-}1)]P(SE), \quad (26)$$

$$P_e = \frac{M/2}{M-1}\left[1-\left\{\int_{-\infty}^{+\infty}\frac{1}{\sqrt{2\pi}}e^{-(w-\sqrt{4K_s})^2/2}dw[1-Q(w)]^{M-1}\right\}\right] \quad (27)$$
$$= \frac{M/2}{M-1}\left[1-\left\{\int_{-\infty}^{+\infty}\frac{1}{\sqrt{2\pi}}e^{-(w-\sqrt{4K_s})^2/2}dw\left[\frac{1}{2}-\frac{1}{2}erf\left(\frac{w}{\sqrt{2}}\right)\right]^{M-1}\right\}\right].$$

For heterodyne detection the bit error probability can be expressed as

$$P_e = \frac{M/2}{M-1}\left[1-\left\{\int_{-\infty}^{+\infty}\frac{1}{\sqrt{2\pi}}e^{-(w-\sqrt{2K_s})^2/2}dw\left[\frac{1}{2}-\frac{1}{2}erf\left(\frac{w}{\sqrt{2}}\right)\right]^{M-1}\right\}\right]. \quad (28)$$

A simple bound often applied in block detection analysis is the union bound. The probability of a finite union of events is bounded above by the sum of the probabilities of the constituent events. Since the binary test between any two decoding symbols is equivalent to an orthogonal coherent test, Eqs. (29) and (30) are obtained.

Following [10], the union bound for the case of homodyne detection is

$$P_e \cong \left(\frac{M}{2}\right)\left[Q[\sqrt{2K_S}\right] = \left(\frac{M}{2}\right)\left\{\frac{1}{2}erfc\left[\sqrt{K_S}\right]\right\}. \quad (29)$$

Similarly, the union bound for the bit error probability for heterodyne detection becomes

$$P_e \cong \left(\frac{M}{2}\right)Q\left[\sqrt{K_S}\right] = \left(\frac{M}{2}\right)\left\{\frac{1}{2}erf\left[\sqrt{\frac{K_s}{2}}\right]\right\}. \quad (30)$$

Figs. 1 and 2 show the exact bit error probabilities and union bound approximation for optical heterodyne and homodyne detection of PPM signals with M=2, 4, 8, 16 slots. Note that, as M increases the bit error probability is higher because we are plotting versus the average number of photons per pulse and not per bit.

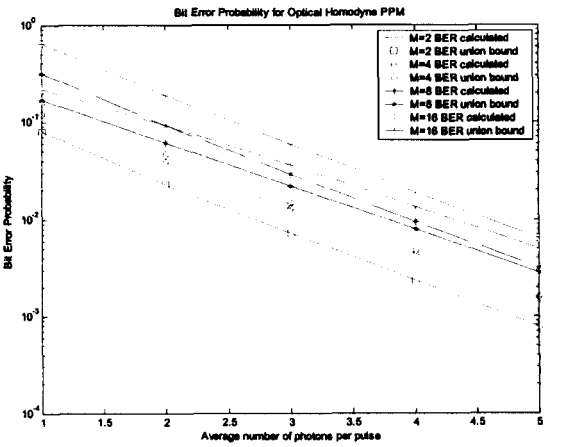

Fig 1. BER for optical homodyne detection.

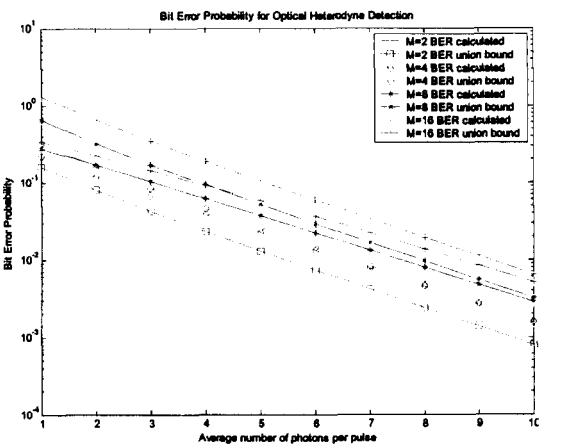

Fig. 2. BER for optical heterodyne detection.

3. EXPERIMENTAL RESULTS AND ANALYSIS

The experimental setup of the optical coherent combining experiment consists of two Nd:YAG lasers operating at 1064 nanometers, whose outputs are aligned and combined on the surface of a 4X4 Fermionics InGaAs detector array, plus an external

electro-optic modulator, a beam expander and other optical elements, 16 RF amplifiers, and a data acquisition assembly as it is shown in Fig. 3. One of the lasers serves as a local oscillator (high output power, 50 mW), while the other simulates the received signal (2-3 mW output). The two lasers are operated at slightly different wavelengths, yielding a relatively stable difference-frequency tone of approximately 6 MHz in the detected signal. The difference-frequency tone is generally observed in several array elements simultaneously, but usually with different phases. If the detector element outputs were simply summed, the addition of out-of-phase signals could result in significant cancellation, yielding a weak signal tone at the output. Non-coherent addition of signal components from different elements of the detector array is analogous to detection with a single large detector: this is the prime reason why a single large detector is not effective for coherent detection of signal fields under turbulent conditions. However, if small areas of the detector surface over which the signal field is essentially coherent are processed separately, then the outputs can be phase-aligned prior to addition, recovering the lost signal power.

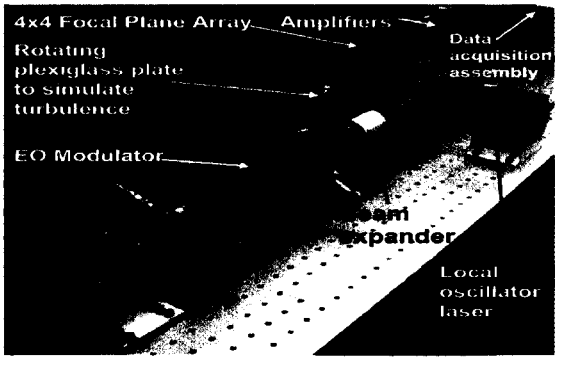

Fig. 3. Coherent combining experiment at the Jet Propulsion Laboratory, NASA.

In the current coherent combining experiment, each of the 16 outputs of the detector array are amplified, and input to a 16-channel data-acquisition assembly (using GaGe data-acquisition cards). The analog signals are digitized to 8 bits at a sampling rate of 25 mega-samples per second (MSPS). The data-acquisition system is capable of synchronously recording up to 1 megabyte of data per channel (or one million 8-bit samples), however we have elected to work with only 104128 samples per channel for these tests, in order to simplify the data-transfer from the data-acquisition computer to the signal-processing computer. At a sampling rate of 25 MSPS, this sample-stream represents 4.16512 ms of elapsed time. Four channels that contained significant signal were identified, and at a certain time synchronously 104128 samples were collected from each channel (in a realistic communications scenario, the combining algorithm would automatically select the "signal" pixels for processing). The modulation format for the transmitted laser signal is PPM using an external electro-optic Modulator (Pockle cell). At the GaGe scope we can see the PPM modulated beatnotes (Fig. 4) at a rate of 97.65 kHz. The PPM frame period is exactly 10.24 μs.

Fig. 4. PPM Beatnotes plus lower frequency oscillation observed using the GaGe Scope data acquisition assembly.

A more detailed snapshot of an individual pulse that contains the coherently detected PPM beatnote is shown in Fig. 5. The pulse width is approximately 300ns for this case, and therefore a 32-PPM system is obtained.

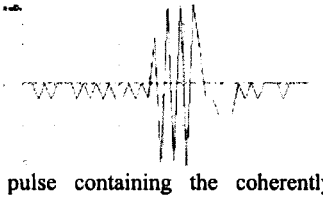

Fig. 5. PPM pulse containing the coherently detected beatnote.

The nominally 6 MHz signal-tones in the presence of simulated atmospheric turbulence were downconverted to complex baseband, and input to a least-mean-square algorithm, or LMS. This adaptive algorithm automatically estimates the complex weights required to reconstruct the signal, then it applies the weights to the complex signal in each channel, and combines the "phased-up" signals in order to maximize power, or SNR. A rotating pre-distorted plexiglass plate was incorporated to simulate atmospheric turbulence. Intensity distribution of the signal beam at the input to the focal-plane array without simulated turbulence is shown in Fig. 6.

Fig. 6. Beam profile of the signal laser with ideal conditions (no atmospheric turbulence).

3.1. The LMS Algorithm

The discrete complex version of the LMS algorithm can be described by the following recursive equation [13], [14]

$$\omega_{P_i}(n+1) = \omega_i(n) + \mu x_i^*(n)\varepsilon(n). \quad (31)$$

The LMS is a recursive algorithm that allows the value of each weight ω_{P_i} at the (n+1) sample to be calculated form its value at the nth sample, using the signals at the nth sample. The sampled error signal in Eq. (32) is obtained from the sampled reference signal and array output, as follows

$$\varepsilon(n) = r(n) - s(n) = r(n) - \sum_{j=1}^{N} \omega_{P_j}(n) x_{P_j}(n). \quad (32)$$

We begin by briefly reviewing the initial experiments using a signal-tone operating with ideal conditions (no atmospheric turbulence added). Secondly, the results of the experiments with a signal-tone in the presence of simulated turbulence conditions will be further explained.

Considering initially the case of ideal conditions, the reference signal used in the algorithm is a constant value calculated based on the addition of the magnitude of the signal in the four channels, which resulted in a value of 0.06 (Fig. 7). As a result, the error signal obtained is a complex number that contains the phase information required. The error signal has to be minimized in order for the phase weights to converge; at that point, the four signals will be phased up and the combined output will be maximized. The weights are computed from Eq. (31) starting with zero initial values. Varying the stepsize, it is possible to control what fraction of the latest weight estimate is applied to the current weight during each update, providing additional smoothing to the weight estimates.

Small stepsize tends to produce good weight estimates under static conditions, however generally leads to greater "weight misadjustment" under dynamic conditions (such as severe Doppler, or severe differential drift between local and signal wavelengths) as the weight estimates cannot keep up with the dynamics. Therefore, there is typically a best stepsize to use for each situation. After some experimentation, it was determined that for this data-set good results could be obtained by correlating over 10,000 samples, and using a stepsize of 1,000. After approximately 30 samples, the weights converge as maximum combined power and minimum error are obtained; that translates to 1.2μs of acquisition time.

Previsouly obtained data have shown that for small values of stepsize (μ=10), the LMS algorithm cannot keep up with the phase variations in the beatnote the combining output signal where the four channels are not perfectly combined as it oscillates and never reaches its maximum value of 0.06. The error signal never settled down to a small value. As the value of the stepsize was increased, with μ=100, performance was greatly improved. The combined output increased in value approaching its maximum. The error signal decreased, showing partial convergence of the weights. Finally, when the stepsize is large enough so that the LMS algorithm is able to keep up with the phase-rotation of the complex downconverted beatnote, at μ=1000, as it is shown in fig. 7, the combined output signal reached its expected maximum value of 0.06.

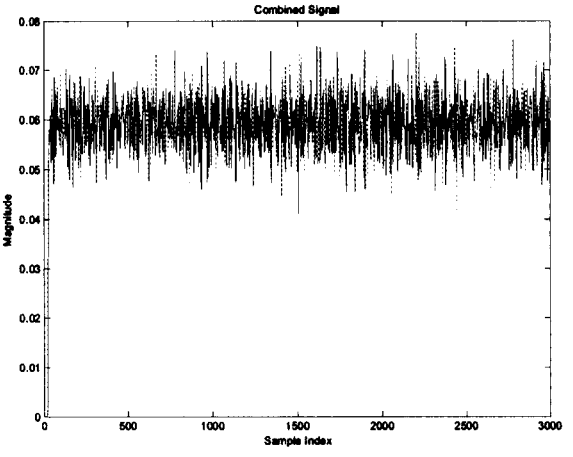

Fig. 7. Combined output power with μ=1000.

With this optimum value of μ, the error approaches zero (Fig. 9) and it is concluded that the signals are phased up. Fig. 8 shows the phase of the weights; the weights have a sawtooth shape, which is due to continuously changing phase in the downconverted output, which is not exactly at zero frequency, but very close to it.

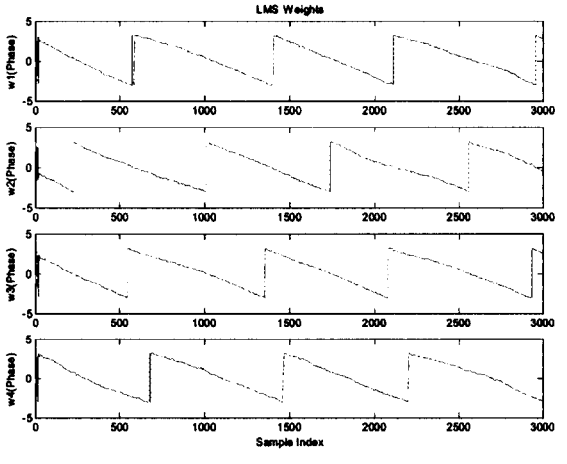

Fig. 8. Phase of the weights for μ=1000.

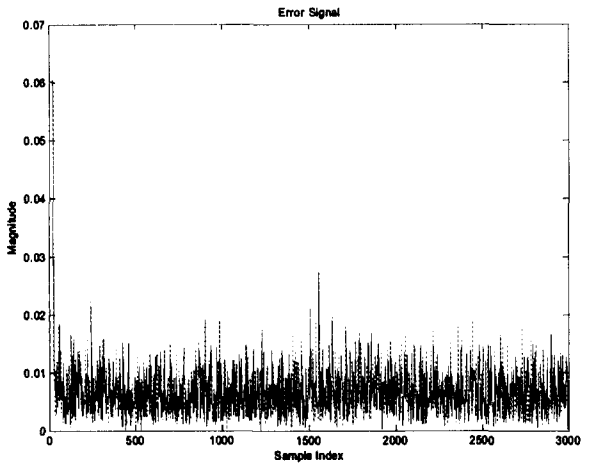

Fig. 9. Error signal with μ=1000.

Now the purpose is to analyze the case of a signal-tone received in the presence of simulated atmospheric turbulence conditions using the rotating plexiglass plate shown in Fig. 3. Fig. 10 represents the intensity distribution of the signal beam in the presence of simulated turbulence conditions.

Fig.10. Intensity distribution of the signal laser in the presence of simulated atmospheric turbulence conditions.

The reference signal used in the algorithm for this situation resulted in a value of 0.0036 (Fig. 11). As in our previous case, four channels that contained significant signal were identified, and at a certain time 104128 samples were synchronously collected from each channel. After some experimentation, it was determined that for this data-set good results could be obtained by correlating over 10,000 samples, and using a stepsize of 20,000 as the signal is even weaker than for the ideal case due to the loss introduced by the atmospheric turbulence added to the system. Fig. 11 shows the combined output that reaches its maximum value of 0.0036. Convergence of the LMS algorithm is accomplished after 200 samples, and therefore the acquisition time is 8 μs.

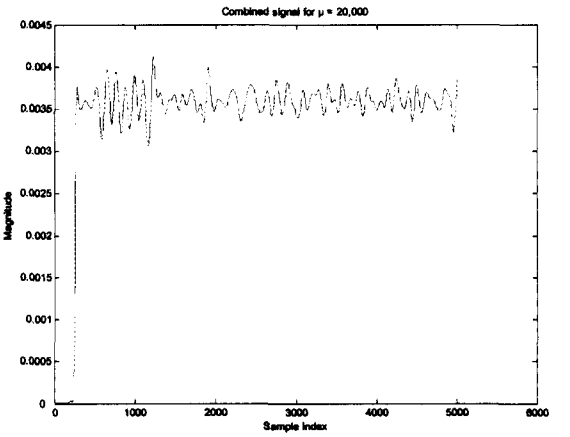

Fig. 11. Combined output power of the beatnote signal in the presence of simulated atmospheric turbulence with μ=20,000.

In order to minimize higher frequency noise contributions in this case, we use a narrower filter bandwidth on the signal processing block.

Fig. 12 shows the phase of the weights with μ=20,000. For this case, the weights also have a sawtooth shape, due to continuously changing phase in the downconverted output, as it is not exactly at 0 Hz.

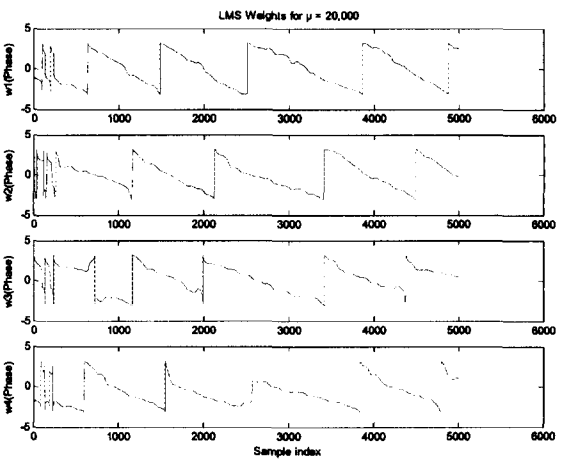

Fig. 12. Phase of the weights with μ=20,000.

Fig. 13 shows the error signal that approaches zero when the stepsize is μ=20,000. Therefore we have accomplished convergence of the LMS and obtained maximum combined output value with minimum error.

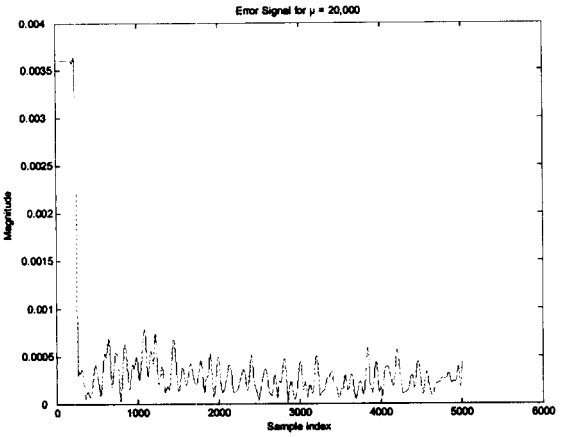

Fig. 13. Error signal with μ=20,000.

These results illustrate, that increasing the stepsize allows the LMS algorithm to follow and track the phase-rotation of the complex downconverted beatnote in the presence of atmospheric turbulence conditions. It was found that a good value of μ for the particular case discussed here is 20,000 when there is accurate tracking of the signals and accordingly, the error signal approaches zero, and maximum combined output is achieved. It is important to note that usually books and papers, the stepsize is shown to be much smaller than one, but that is because the signal is assumed to be of unity amplitude. In our experiment, the signal levels that we are dealing with are very small as there is not enough amplification after detection. Therefore, large values of stepsize are needed to provide adequate updates to the weights.

4. CONCLUSIONS AND FUTURE WORK

We have been able to track the phase of the beatnote signals in the presence of simulated atmospheric turbulence coming out of the photodetector using the LMS algorithm producing an optimum combined signal output. We have modulated the signal with PPM maintaining the pulse-to-pulse coherence of the optical fields (because of the external modulator) enabling the use of the LMS. We plan to conduct detection measurements of the PPM beatnotes in order to compare the experimental results with the theoretically homodyne and heterodyne curves obtained. It has to be mentioned too, that as we relax the requirements for inter-pulse coherence, there will be a need to use other combining algorithms that do not depend on temporal coherence on a short time-scale, such as suitably modified versions of a "constant modulus algorithm" (CMA) or other appropriate algorithms that we will develop to work also under turbulent conditions.

5. ACKNOWLEDGMENTS

The authors would like to acknowledge Carlos Esproles for his help on the laboratory setup and Angel Portillo for his simulations contributions.

REFERENCES

1. R. M. Gagliardi, S. Karp, "Optical Communications," 2nd ed., Wiley Series in Telecommunications and Signal Processing, New York, 1995, Chapter 5.
2. M. Bass, (editor in chief), "Handbook of Optics, Fiber Optics and Nonlinear Optics," 2nd ed., Vol. IV, McGraw-Hill, New York, 2001, Chapter 1.
3. J. C. Palais, "Fiber Optic Communications," Prentice Hall, New Jersey, 1998, Chapter 10.
4. G. R. Osche, "Optical Detection Theory for Laser Applications," Wiley Series in Pure and Applied Optics, New Jersey, 2002, Chapter 1.
5. A. Yariv, "Optical Electronics," Holt, Rinehart and Winston, Inc., 1985, Chapter 11.
6. S. B. Alexander, "Optical Communication Receiver Design," The Society of Photo-Optical Instrumentation Engineers, 1997, Chapter 3.
7. C. N. Georghiades, D. L. Snyder, "Receiver Performance for Heterodyne Optical Communication," IEEE Transactions on Communications, Vol. Com-34, No. 11, November 1986.
8. R. M. Gagliardi, S. Karp, "Optical Communications," 2nd ed., Wiley Series in Telecommunications and Signal Processing, New York, 1995, Chapter 6.
9. V. A. Vilnrotter, "An M-ary Coherent Optical Receiver for the Free-Space Channel," TDA Progress Report 42-66, Jet Propulsion Laboratory, Pasadena, September and October 1981.
10. J. M. Wozencraft, I. M. Jacobs, "Principles of Communication Engineering," John Wiley & Sons, Inc., New York, 1965, Chapter 4.
11. A. J. Viterbi, "Principles of Coherent Communications," McGraw-Hill Book Company, New York, 1966, Chapter 8.
12. V. A. Vilnrotter, M. Srinivasan, "Adaptive Detector Arrays for Optical Communications Receivers," IEEE Transactions on Communications, Vol. 50, No. 7, July 2002.
13. B. Widrow, S. D. Stearns, "Adaptive Signal Processing," Prentice-Hall Signal Processing Series, Prentice-Hall Inc., New Jersey, 1985, Chapter 6.
14. R.T. Compton, Jr., "Adaptive Antennas," Prentice-Hall Inc., New Jersey, 1988, Chapter 2.